**Naval Research Laboratory**

**Washington, DC 20375-5320**

**NRL/MR/6790--13-9450**

# Development of a High Average Current Thermionic Injector for Free-Electron Lasers

S.H. GOLD
A. TING

*Beam Physics Branch*
*Plasma Physics Division*

V. JABOTINSKI

*Beam-Wave Research, Inc.*
*Bethesda, Maryland*

P. SPRANGLE

*Directed Energy Physics*
*Plasma Physics Division*

February 11, 2013

# REPORT DOCUMENTATION PAGE

Form Approved
OMB No. 0704-0188



| 1. REPORT DATE *(DD-MM-YYYY)* | 2. REPORT TYPE | 3. DATES COVERED *(From - To)* |
|---|---|---|
| 11-02-2013 | Interim | November 2011 – November 2012 |

**4. TITLE AND SUBTITLE**

Development of a High Average Current Thermionic Injector for Free-Electron Lasers

**5a. CONTRACT NUMBER**

**5b. GRANT NUMBER**

**5c. PROGRAM ELEMENT NUMBER**

**6. AUTHOR(S)**

S.H. Gold, A. Ting, V. Jabotinski,[1] and P. Sprangle

**5d. PROJECT NUMBER**
67-4570-02

**5e. TASK NUMBER**

**5f. WORK UNIT NUMBER**

**7. PERFORMING ORGANIZATION NAME(S) AND ADDRESS(ES)**

Naval Research Laboratory
4555 Overlook Avenue, SW
Washington, DC 20375-5320

**8. PERFORMING ORGANIZATION REPORT NUMBER**

NRL/MR/6790--13-9450

**9. SPONSORING / MONITORING AGENCY NAME(S) AND ADDRESS(ES)**

High Energy Laser
Joint Technology Office
801 University Blvd. SE, Suite 209
Albuquerque, NM 87106

**10. SPONSOR / MONITOR'S ACRONYM(S)**

JTO

**11. SPONSOR / MONITOR'S REPORT NUMBER(S)**

**12. DISTRIBUTION / AVAILABILITY STATEMENT**

Approved for public release; distribution is unlimited.

**13. SUPPLEMENTARY NOTES**

[1]Beam-Wave Research, Inc., 5406 Bradley Boulevard, Bethesda, MD 20814

**14. ABSTRACT**

Thermionic electron guns are capable of operating at high average currents in a variety of vacuum electronic applications, including conventional microwave tubes, but have been replaced by laser photocathode injectors for most free-electron laser (FEL) applications. However, while laser photocathode guns are capable of providing the very high brightness beams required for short wavelength FELs, they provide an increased level of system complexity and do not extrapolate well to injectors for high average current FEL applications. We are developing a 700 MHz injector based on a gridded thermionic electron gun for this application. This paper presents an experimental study, computer simulations, and analysis of the performance of an existing gridded thermionic electron gun as an injector prototype, and a design concept for an improved injector configuration based on these results.

**15. SUBJECT TERMS**

Free electron lasers
Thermionic gun
RF gated thermionic cathode
High average beam current

| 16. SECURITY CLASSIFICATION OF: | | | 17. LIMITATION OF ABSTRACT | 18. NUMBER OF PAGES | 19a. NAME OF RESPONSIBLE PERSON |
|---|---|---|---|---|---|
| a. REPORT | b. ABSTRACT | c. THIS PAGE | | | Steven H. Gold |
| Unclassified Unlimited | Unclassified Unlimited | Unclassified Unlimited | Unclassified Unlimited | 24 | 19b. TELEPHONE NUMBER *(include area code)* (202) 767-4004 |

# Development of a High Average Current Thermionic Injector for Free-Electron Lasers

S.H. Gold, A. Ting, V. Jabotinski[1], and P. Sprangle

Plasma Physics Division
Naval Research Laboratory, Washington, DC 20375

[1] Beam-Wave Research, Inc., Bethesda, MD 20814

## Abstract

Thermionic electron guns are capable of operating at high average currents in a variety of vacuum electronic applications, including conventional microwave tubes, but have been replaced by laser photocathode injectors for most free-electron laser (FEL) applications. However, while laser photocathode guns are capable of providing the very high brightness beams required for short wavelength FELs, they provide an increased level of system complexity and do not extrapolate well to injectors for high average current FEL applications. We are developing a 700 MHz injector based on a gridded thermionic electron gun for this application. This paper presents an experimental study, computer simulations, and analysis of the performance of an existing gridded thermionic electron gun as an injector prototype, and a design concept for an improved injector configuration based on these results.

## 1. Introduction

RF linear accelerators are used to accelerate short bunches (microbunches) of electrons using the rf fields excited in standing-wave or traveling-wave structures. The quality and bunch length of the electrons injected into the first rf cell are critical to the properties of the final high energy electron bunches that are generated by a complete accelerator system [1]. When the application is to the generation of electromagnetic radiation in a free-electron laser, the final beam quality requirements in the interaction region can be traced back to requirements on the electron microbunches injected into the first cell of the rf accelerating system. For the FEL application, the initial electron bunches are typically generated using a photocathode excited by laser irradiation [2–9]. However, this is an expensive approach that does not easily scale to robust systems requiring high average beam currents. Another approach is to employ thermionic electron guns [10–16]. In this paper, we evaluate the potential of a gridded thermionic electron gun as the first stage of an injector system for an accelerator for a near infrared free-electron laser.

The plan of our program is to carry out experimental measurements and theoretical investigations on a commercially available gridded thermionic electron

Manuscript approved December 12, 2012.

gun driven at ~700 MHz, and to study electron bunch length, bunch charge, and transverse beam emittance as a function of negative grid bias and rf drive power at gun voltages of 30–35 kV. Also, we want to test the effects of adding third harmonic drive to the cathode-grid circuit to reduce the electron bunch length. These measurements are then compared to simulations using the electron gun code MICHELLE [17] in order to model the diagnostics and to benchmark the simulations. MICHELLE simulations are also used to study an alternative electron gun design that can have improved transverse emittance and shorter electron bunch length.

## 2. Requirements for the electron gun

The electron injector for a high average power FEL should produce high charge electron bunches with low energy spread ready for injection to the RF linac. Typical beam parameters for such an injector are a bunch charge of ~1 nC at a repetition rate of ~700 MHz in CW operation. P. Sprangle and coworkers [18] showed that the energy spread of the particle bunches in the interaction region of an FEL has three major contributing components due to the transverse emittance, the longitudinal emittance, and the wiggler gradients and derived an equation describing the resulting energy spread

$$\frac{\Delta \mathrm{E}}{\mathrm{E}} = \frac{\varepsilon_{\perp}^2}{2r_b^2} + \frac{\varepsilon_{\parallel}}{\tau_b E} + \frac{\pi^2}{2}\left(\frac{a_w}{\lambda_w} r_b\right)^2 \quad , \qquad (1)$$

where $\varepsilon_{\perp}$ is the bunch normalized transverse RMS emittance, $\varepsilon_{\parallel}$ is the bunch normalized longitudinal RMS emittance, $r_b$ is the bunch RMS radius, $\tau_b$ is the RMS bunch duration, and $\lambda_w$ and $a_{\mathrm{w}}$ are the wiggler period and wiggler parameter, respectively.

Based on (1), we can derive the requirements for the electron injector and for the RF-gated bunched thermionic electron gun to be: transverse normalized RMS emittance of $\varepsilon_{\perp}$ < 15 mm mrad, longitudinal normalized RMS emittance of $\varepsilon_{\parallel}$ < 100 kV ps, and bunch RMS duration of $\tau_b$ < 50 ps.

## 3. Experimental setup

The goal of the experiment is to characterize the performance of a gridded thermionic electron gun from Communications and Power Industries, Inc. (CPI) that is similar to the electron gun used in the production of inductive output tube amplifiers (IOTs) [19]. The gun has been modified somewhat and ends in an output flange rather than connecting to an IOT output cavity. The gun incorporates a dispenser cathode and a pyrolytic graphite grid that can modulate the cathode emission at frequencies greater than 1 GHz. In an IOT, the modulated electron beam would then interact in a resonant output cavity in order to generate tens of kilowatts of rf power at the drive frequency at up to 100% duty factor. Here, the gun is being used as the prototype of an advanced thermionic gun that will be

optimized for minimum bunch length and minimum normalized emittance while operating at ~1 nC microbunch charge in fully cw operation at ~700 MHz.

The electron gun includes a 3-cm diameter cathode and a closely spaced pyrolytic graphite grid that is biased negatively with respect to the cathode. The center of the cathode is ~5 cm from the end of the output flange. A central hole ~7 mm in diameter passes through the cathode and the grid wires, and is intended to reduce cathode damage due to ion back bombardment. As part of an IOT, the electron gun would normally operate with negative DC high voltage on the cathode, with the emission controlled by the grid bias and the rf drive. However in our experiment, the cathode-grid circuit is pulsed to a negative high voltage of up to -36 kV using a high voltage modulator. The cathode heater is powered by a 60 Hz AC feed that floats on the high voltage pulse, and an adjustable negative grid bias of up to –180 V also floats with the high voltage pulse. The negative bias on the grid, which suppresses electron emission, is combined with direct rf modulation of the cathode-grid circuit via a coaxial feed line to produce a high-current electron beam that is bunched at the rf frequency. The goal of our experiments is to characterize the properties of the electron beam, first by depositing the electrons in a Faraday cup placed close to the output flange, in order to measure the temporal width and charge of electron bunches, and second by using slit-based optical measurements to determine the electron beam emittance.

The high-voltage power supply for the IOT gun is a 70 kV Rockwell hard tube modulator with an output pulse width that is variable up to ~15 μs. For these experiments, the voltage was limited to ~36 kV and the output pulse width was set at its maximum. The heater coil inside the cathode assembly is not compensated by a center return. As a result, it produces stray magnetic fields at the cathode surface that oscillate at 60 Hz, producing a variation in the beam from the gun. In order to avoid this effect, the modulator timing was synchronized with the zero crossing of the heater current measured at the cathode. Experimental measurements were typically performed late in the pulse, in order to minimize the effect of gun turn-on transients and voltage ringing. In the case of rf drive, a 1-μs rf pulse was applied to the grid circuit using the same timing near the end of the high voltage pulse, and fast timescale measurements were made in a window within the rf pulse.

Figure 1 shows the experimental setup used to measure the length and charge of the electron bunches from the gun. The rf drive for the cathode-grid circuit was produced by a Technical Services Laboratory Model 1710 dual frequency amplifier that provides up to ~500 W of output at a fundamental frequency tunable between 700 MHz and 714 MHz as well as up to ~450 W at the third harmonic of the fundamental frequency, with both signals combined in a single coaxial line. Both output signals are locked to a single 100 kHz crystal oscillator, with separate controls of the two output power levels as well as control of the relative phase between the fundamental and third harmonic signals. The output power levels are read out directly from the amplifier using an internal peak power meter, and the rf is also monitored using a bidirectional coupler that is read out directly on a fast digital oscilloscope. The cathode-grid circuit is fed by a 50 ohm Heliax cable. The coaxial feed from the amplifier employs separate low and high frequency slug tuners

for impedance matching into the electron gun. For reasons of convenience, we chose to carry out these experiments at 714 MHz and 2142 MHz.

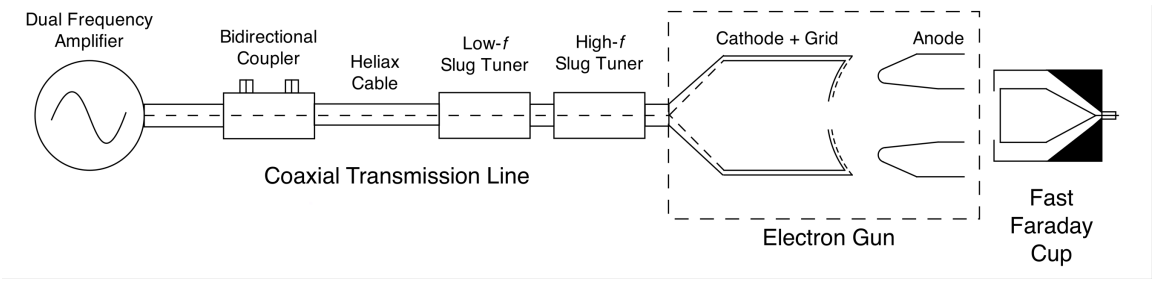


Fig. 1. Schematic diagram of the experimental setup for bunch length measurements.

The electron bunches from the gun were collected on the copper cone of a fast Faraday cup (Princeton Scientific Corp.) with ~50 ps time resolution. The Faraday cup includes a grid that is biased negative with respect to the copper cone in order to capture secondary electrons generated by the impact of beam electrons on the copper cone. The Faraday cup was placed as close as possible (~3 cm) to the gun output flange in order to limit bunch spreading due to velocity spread and space charge effects. The current collected by the Faraday cup passed through calibrated attenuators and was recorded by a Tektronix DSA 71604B 16-GHz digital oscilloscope, with the signal line terminated in 50 ohms. The experimental variables were the gun voltage, the grid bias voltage, and the level of fundamental and third harmonic rf drive. In addition, the heater power was controlled to ensure reproducible emission from the cathode.

## 4. Discussion of the Faraday cup data

Figure 2 shows the measured current from the Faraday Cup as a function of negative grid bias with -31 kV of pulsed high voltage on the cathode. The peak current at 0 V grid bias is ~2.5 A, which according to our simulations corresponds to mixed space-charge and temperature-limited emission from the cathode. However, as the negative grid bias is increased, the emission from the cathode becomes space-charge limited, and falls rapidly until about -70 V. Simulations show that emission from the face of the cathode through the grid should cut off sharply at this value of grid bias. However, the experimental data shows that the emission does not cut off at this value of negative grid bias. Instead, it continues to fall steadily, but at a slower rate than at lower values of grid bias, and there is still 3.6 mA of current at -126 V grid bias. This behavior indicates that there is a source of unwanted emission in the gun that is not effectively controlled by the grid bias.

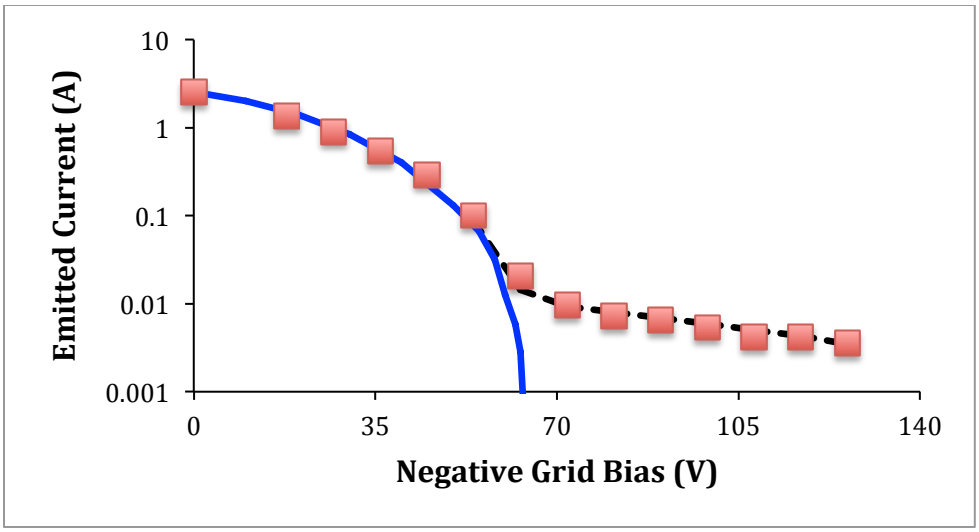


Fig. 2. Measured beam current versus negative grid bias for $V_{cathode}$=−31 kV. The solid line is from a MICHELLE simulation of the electron gun, with emission only from the face of the cathode. The simulation model takes into consideration temperature-limited emission from the cathode at 1095K. The dashed line includes emission from both the face of the cathode and the edge surface of the central hole through the cathode.

One possible source of the unwanted emission is emission from the grid wires, which can become contaminated with barium from the hot cathode and may be hot enough to emit. However, this explanation is not well supported by the data, which shows that the emission continues to fall monotonically as the grid bias is increased above the predicted cut-off value. Emission from the grid wires should not be affected in this way by the grid bias, since the change in voltage between the grid and anode is less than 1%.

The second possibility is emission from the edge surface of the central hole through the cathode, which can readily be contaminated with barium, and which is clearly hot enough to emit. Electron trajectories originating in this region and leaking through the central hole in the grid wires would still be affected by the grid potential, though to a lesser extent than emission from the face of the cathode, and should decrease monotonically as the negative grid bias is increased. This mechanism explains the data in Fig. 2, as shown in the dashed curve that is derived from a simulation that includes emission from the edge surface of the central hole through the cathode, and it also sheds light on the results of rf-gated Faraday cup measurements that are shown in later figures. In addition, further evidence of this phenomenon based on optical diagnostics will be presented later in this paper.

The phenomenon of current escaping through the central hole in the grid wires was discussed by E. Wright and coworkers in [20] as the source of interbunch emission in the presence of rf grid drive, based on their MICHELLE simulations of a similar IOT electron gun. In the context of an IOT amplifier, this phenomenon will result in some electrons entering the output cavity in the accelerating phase of the cavity fields, and gaining energy as they transit the output cavity, resulting in x-ray production when they are deposited in the IOT collector. However, Ref. [20]

analyzed interbunch current only in the presence of rf drive. Our results, as well as the corresponding MICHELLE simulations, in which the edge of the cathode hole is permitted to emit, show that there is also a dc component of current emerging from the center hole with no rf drive and in the presence of strong negative grid bias.

In the IOT application, the gridded electron gun is typically used to create ~180 degree modulation of the electron beam, in order to efficiently generate high power rf in the output cavity [21]. However, the injector application requires the generation of much shorter electron bunches for injection into the optimum phase of a set of rf accelerating cavities. In the presence of a negative grid bias combined with a single frequency rf drive, the cathode will emit electrons whenever the instantaneous grid bias is positive. As a result, the length of the electron bunches can be controlled by the ratio of the peak rf amplitude applied to the grid and the value of the negative grid bias. This simple picture ignores transit-time effects in the cathode-grid gap. Nevertheless, as that ratio is decreased towards one, the bunch lengths are reduced, the peak bunch current is reduced, and for both reasons, the charge per bunch is also reduced.

One means to reduce the bunch length without simultaneously reducing the peak bunch current is to change the rf modulation waveform from sinusoidal to a more peaked waveform. One practical way to accomplish this is to add higher harmonic modulation to the grid drive. We chose to investigate third harmonic modulation, in this case at 2142 MHz, that is locked in phase with the fundamental harmonic modulation at 714 MHz. With the correct relative phase between the two signals, the rf modulation will become more peaked, and thus shorter bunches will in principle be produced at the same peak rf amplitude on the grid. In order to carry out this procedure, a special dual-frequency amplifier was purchased for this experiment, as described earlier in this paper.

One experimental question that needed to be addressed was to establish that the 2142 MHz signal at the input to the electron gun would cause effective rf modulation of the voltage across the cathode-grid gap. Figure 3 addresses this issue. It shows the measured Faraday cup waveforms corresponding to single-frequency modulation at 714 MHz and 2142 MHz. The 714 MHz rf modulation of the grid produces strong modulation of the current measured by the Faraday cup, with a peak current of ~2.2 A and 0.9 nC per bunch. However, there is also evidence of interbunch current, as indicated by the downward shift of the signal from the baseline of the trace, which is indicated by the pink dot on the left axis. This current is believe to be related to the unmodulated current emitted from the central cathode hole, as discussed with reference to Fig. 2. The 2142 MHz modulation also produces a modulation of the current measured by the Faraday cup, thus demonstrating that the 2142 MHz modulation is appearing across the cathode-grid gap. However in this case the dc component, or interbunch current, is much larger than the modulated current. In this case, the baseline of the trace is indicated by the green dot on the left axis. This less effective bunching may be due to transit-time effects in the gap between the cathode and grid. Also, the peak microbunch current of 110 mA is substantially lower than the 2.2 A current measured at 714 MHz, even though the negative grid bias is lower and the rf drive is substantially higher. In addition to

possible transit-time effects, this appears to be due to the less effective coupling of rf power into the cathode-grid gap.

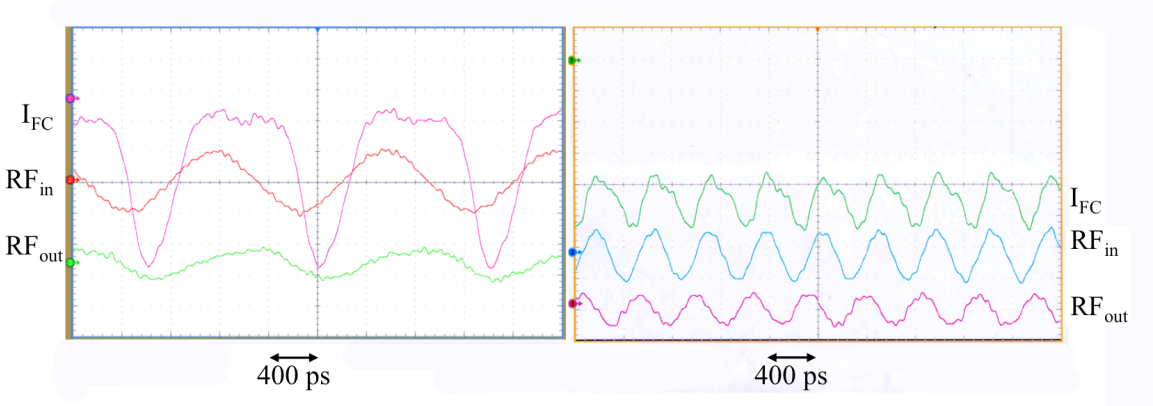


Fig. 3. Measured Faraday cup current ($I_{FC}$) for single-frequency 714 MHz (left) and 2142 MHz (right) grid drive. For the left-hand data set, the parameters are $V_{cathode}$=24 kV, $V_{grid}$=-90 V, and ~100 W at 714 MHz producing a 408 ps FWHM (~170 ps RMS) micropulse with peak current ~2.2 A and 0.9 nC per bunch. For the right-hand data set, the parameters are $V_{cathode}$=24 kV, $V_{grid}$=-63 V, and ~300 W at 2142 MHz, producing a peak current of ~110 mA. The colored dot on the left axis associated with each waveform shows the associated baseline of the trace. Also shown are the incident and reflected rf waveforms, $RF_{in}$ and $RF_{out}$.

In order to estimate the effective coupling of an rf signal into the cathode-grid gap, we used a simple model of the rf input circuit as a 50 ohm coaxial transmission line driving a purely capacitive load. (There will also be a resistive component when an electron beam is generated.) The cathode-grid region was modeled as two parallel 3-cm disks separated by 250 μm, resulting in an estimated capacitance of $C$=25 pF. The impedance of the capacitor is then $(i\omega C)^{-1}$, where ω=2π$f$, and $f$ is either 714 MHz or 2142 MHz. In this case, for 100 W of rf drive, the cathode-grid voltage would be approximately 51 V at 714 MHz and 8.5 V at 2142 MHz. These calculations do not include the effect of the slug tuners in the transmission line, which are always adjusted to minimize the reflected signal from the electron gun at both frequencies. However, they do suggest that the effective coupling to the cathode-grid gap will be substantially lower for the third harmonic signal.

The next test was to employ combined modulation of the cathode-grid circuit at both 714 MHz and 2142 MHz. To optimize the combined waveforms, the relative phase of the two single-frequency components was adjusted to produce the shortest effective electron bunch lengths. Figure 4 shows the Faraday cup measurements for $V_{cathode}$=-36 kV, $V_{grid}$=-90 V, with ~540 W at 714MHz and ~450W at 2142 MHz. The microbunches are 325 ps FWHM (~135 ps RMS), with 2.81 A peak current and ~0.91 nC per bunch. Note that RMS bunch durations are calculated assuming a Gaussian waveform with the measured value of FWHM. As noted for the previous data, a small level of DC, or interbunch current, persists.

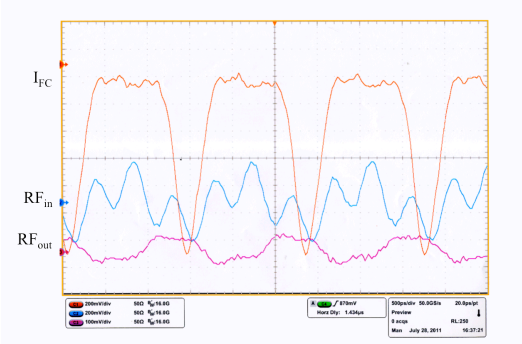


Fig. 4. Measured Faraday cup current, $I_{FC}$, for combined first and third harmonic modulation of the electron gun. The parameters are $V_{cathode}$=-36 kV, $V_{grid}$=-90 V, with ~540 W at 714MHz and ~450W at 2142 MHz. The microbunches are 325 ps FWHM (135 ps RMS), with 2.81 A peak current and ~0.91 nC per bunch. Also shown are $RF_{in}$ and $RF_{out}$.

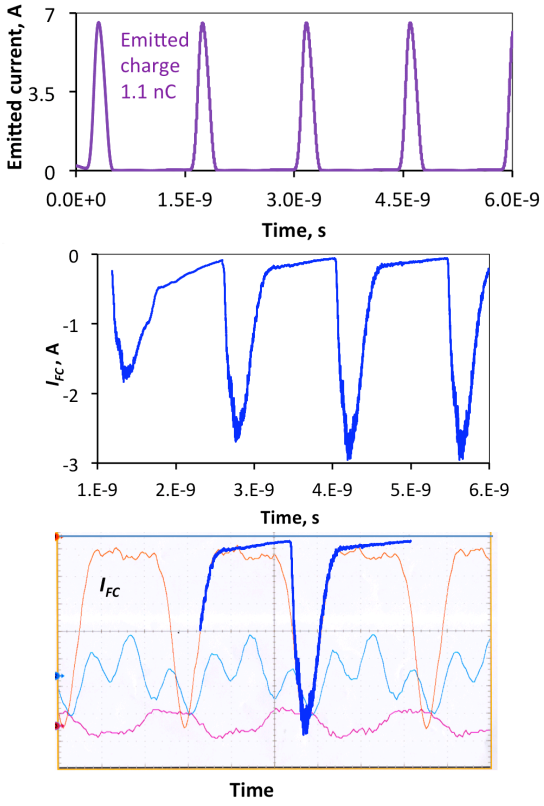


Fig. 5. MICHELLE simulation of the bunched beam for operation corresponding to Fig. 4. (top) Emitted current from the cathode; (center) current reaching the Faraday cup; (bottom) comparison of simulation and experimental data from Fig. 4.

Fig. 5 shows a MICHELLE simulation of the operation of the electron gun for parameters corresponding to Fig. 4, including first and third harmonic rf drive. However, since there is no direct experimental determination of the rf voltages in the cathode-grid gap, these voltages were set to $U_1$=69 V and $U_3$=23 V to provide a good fit to the data. Fig. 5 (top) shows the emission from the cathode, which peaks at more than 6 A, with 1.1 nC charge per bunch. The FWHM of the cathode current

bunch is 160 ps, and the RMS width is 74.7 ps. Fig. 5 (center) shows the bunch shape at the position of the Faraday cup (8 cm from the center of the cathode). Here, the peak bunch current is 2.96 A, with 0.95 nC charge per bunch. Also, the FWHM of the bunch is 301 ps. The RMS bunch width is 160 ps, but is strongly influenced by the tail of the bunch, which corresponds to interbunch current. Note that the first two bunches are not typical, and the bunch is still evolving to the shape shown in the third and subsequent bunches. Fig. 5 (bottom) shows a comparison of the third bunch to the bunches measured in Fig. 4.

One means to shorten the length of the electron bunches is to employ higher values of negative grid bias. Fig. 6 shows data for $V_{grid}$=-100 V (left) and $V_{grid}$=-125 V (right). In order to optimize the bunches, the applied power at 714 MHz was reduced to ~200 W, while the same ~450 W was applied at 2142 MHz. For $V_{grid}$=-100 V, the electron bunches are 235 ps FWHM (~98 ps RMS) and the peak bunch current is 580 mA, corresponding to ~135 pC per bunch. For $V_{grid}$=-125 V, the bunch length is reduced to 190 ps FWHM (80 ps RMS), but the peak bunch current drops to 74 mA, corresponding to only 14 pC per bunch. The rapid fall off of peak bunch current and charge per bunch at higher levels of negative grid bias shows the limitation of this approach when applied to the existing electron gun. However, these measurements also document the capability of the Faraday cup to measure these short bunches, indicating that the measured bunch shapes shown in Fig. 4 should not be broadened by the diagnostics.

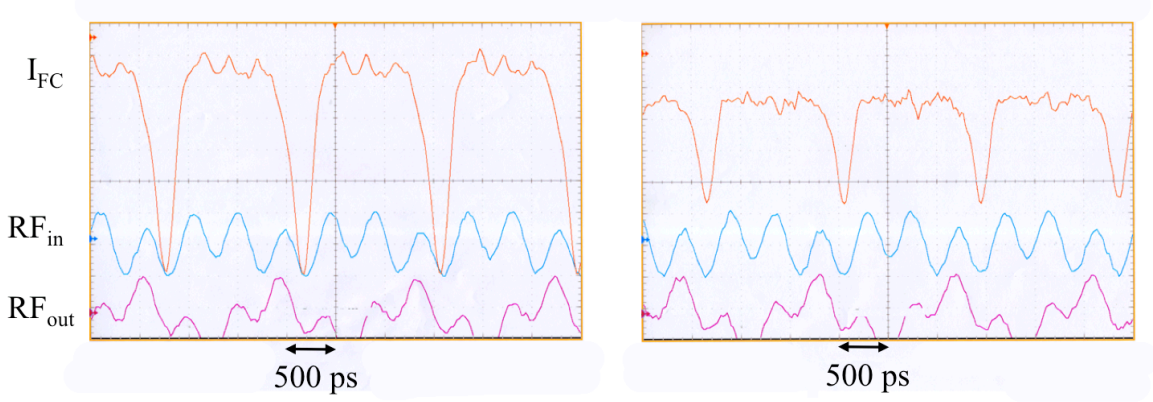


Fig. 6. Faraday cup data for combined first and third harmonic modulation of the electron gun and higher negative grid bias for $V_{cathode}$=-36 kV and ~200 W at 714MHz and ~450W at 2142 MHz. The left traces correspond to $V_{grid}$=-100 V; the right traces correspond to $V_{grid}$=-125 V.

In order to examine the effect of adding 2142 MHz modulation to the grid, we took a set of data at $V_{cathode}$=-36 kV and $V_{grid}$=-117 V in which the peak microbunch current was set to 0.6 A with only 714 MHz modulation applied, and then various levels of 2142 MHz modulation were added, and the 714 MHz modulation decreased, in order to maintain 0.6 A of peak microbunch current. The results are shown in Fig. 7. With no third harmonic drive, approximately 165 W of power at 714 MHz was required, resulting in an RMS bunch width of ~112 ps. The required first harmonic power drops monotonically as the third harmonic power is increased, and is reduced to ~120 W with ~200 W at third harmonic, resulting in a microbunch length of ~96 ps RMS. Neither the first harmonic power required to produce 0.6 A

peak bunch current at this value of negative grid bias nor the RMS bunch length change much when the third harmonic drive is further increased in steps up to ~475 W. This data demonstrates that increasing the ratio of third to first harmonic power can help shorten the RMS length of the electron bunches for a fixed value of the peak microbunch current.

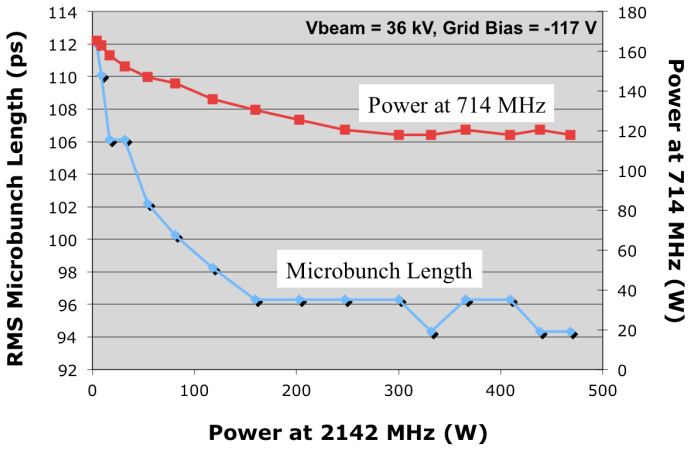


Fig. 7. RMS bunch length and first harmonic power versus third harmonic power at 0.6 A peak microbunch current.

Figure 8 shows a plot of peak microbunch current and microbunch length versus the power applied at 714 MHz with the 2142 MHz power set at ~400 W and the grid bias set to $V_{grid}$=-108 V. Both the bunch length and the peak microbunch current increase as the first harmonic drive power is increased.

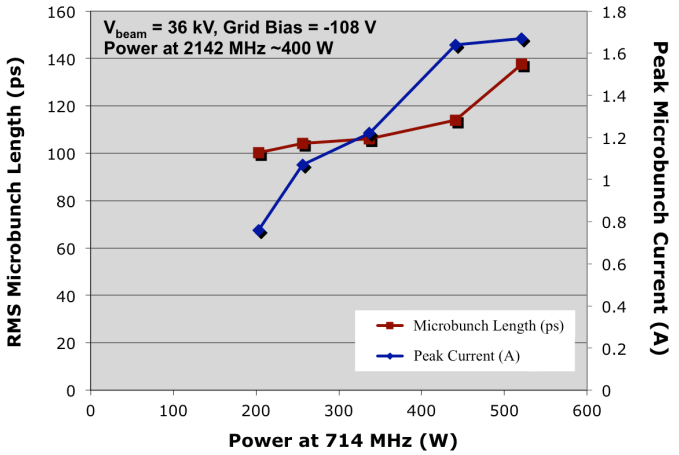


Fig. 8. Peak current and microbunch length versus power at 714 MHz.

## 5. Discussion of the emittance data

Aside from bunch length and bunch charge, the remaining critical parameter for the bunches produced by the electron gun is their transverse emittance. For our low energy beam, we chose to employ a slit-base measurement [22–24], in which a

100 μm horizontal tantalum slit was scanned across the beam using a vertical translator and the electrons passing through the slit were intercepted by a YAG:Ce fluorescent screen. The fluorescent screen was also mounted on a vertical translator, in order to keep it centered on the resulting electron trajectories. In turn, the fluorescent screen was imaged and recorded using a digital CCD camera (FOculus camera model FO531TB) controlled by LABVIEW™ software. The camera was triggered electronically. The exposure time was set to ~3 μs, which permitted the camera to discriminate against emission that did not occur during the typical 1-μs rf drive pulse. The low beam energy and the beam divergence make it difficult to carry out accurate measurements, since the most divergent electron trajectories may intercept the wall of the vacuum vessel before reaching the slit plane, and some trajectories through the slit may also intercept the wall before reaching the YAG screen. Several different experimental setups were used, in an attempt to optimize the acceptance of divergent electron trajectories.

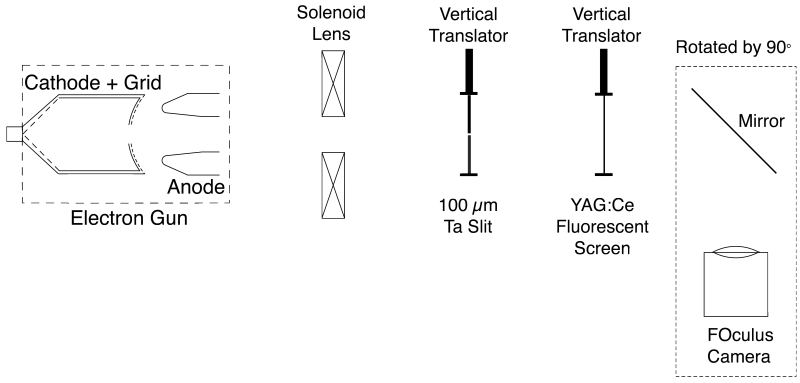


Fig. 9. Schematic of experimental setup for emittance measurements (not to scale). The vacuum enclosure is not shown.

Figure 9 shows a schematic of the final experimental setup that was employed. In this setup, a solenoidal lens was added to help collimate the beam, thus ensuring that more of the beam reached the slit plane, and that more of the electrons that passed through the slit reached the YAG screen. The effective geometry from the gun up to the slit plane is shown in Fig. 10, which also shows a MICHELLE simulation of the electron trajectories from the gun, both without lens current (center), and with a lens current of 1.65 A (top). In these simulations, the gun is modeled for $V_{cathode}$=-32 kV and $V_{grid}$=-90 V with only first harmonic rf drive applied. Since we cannot directly measure the grid modulation amplitude resulting from a particular rf power from the amplifier, the rf modulation of the cathode-grid gap was adjusted in the simulation to produce a peak microbunch charge of ~0.75 nC. Figure 10 shows that even at $I_{lens}$=1.65 A, some electron trajectories are lost to the wall before reaching the slit plane. In examining Fig. 10, it is important to note that the trajectories do not carry equal amounts of charge. Figure 10 (bottom) shows a simulation of the trajectories with no lens current, but with the emission from the edge of the cathode hole suppressed. A comparison of the bottom and

center simulations shows the affect of emission from the edge of the cathode hole in creating interbunch current.

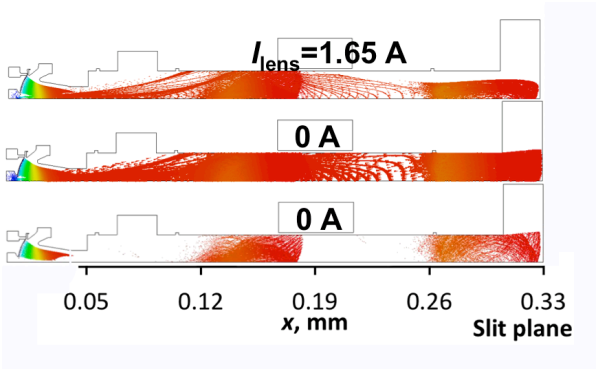


Fig. 10. Simulation of the emission measurements at $V_{cathode}$=-32 kV and effect of the emission from the central hole. Electron trajectories for: (top) $I_{lens}$=1.65 A and (center) $I_{lens}$=0 A include emission from the central hole; (bottom) $I_{lens}$= 0 A is with emission from the central hole suppressed.

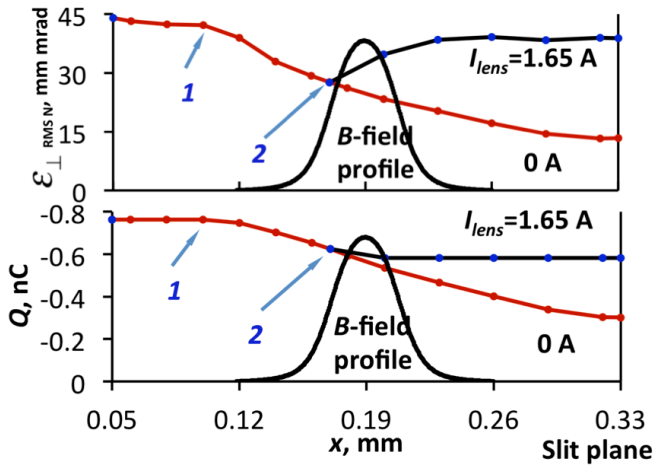


Fig. 11. Simulation of the emission measurements at $V_{cathode}$=-32 kV. Normalized RMS transverse emittance (top) and bunch charge (bottom) as a function of axial position for $I_{lens}$=1.65 A and $I_{lens}$= 0 A. Particles begin hitting the wall at the point labeled 1 and the magnetic field begins to affect the emittance at the point labeled 2. The normalized magnetic field profile of the lens is also shown.

Figure 11 shows simulations of the emission measurements at $V_{cathode}$=-32 kV for $I_{lens}$=1.65 A and $I_{lens}$= 0 A. The upper plot shows the normalized RMS transverse emittance and the lower plot shows the corresponding bunch charge as a function of axial position. At location 1, electrons begins to hit the wall, and as a result the emittance of the bunch begins to drop. However, it is also important to note that the most divergent trajectories originate from the hole through the anode, and correspond to unmodulated emission from the gun, as shown in the bottom simulation shown in Fig. 10. In Section 6, we will discuss the design of a new electron gun configuration that eliminates this central hole, and therefore should eliminate the most divergent trajectories.

The lower plot in Fig. 11 shows that at $I_{lens}$=1.65 A, the solenoidal lens reduces the loss of bunch charge as a function of distance from the gun. This is most apparent downstream from the lens. However, the simulations also predict that the lens itself causes the bunch emittance to increase somewhat, as shown in the upper plot of Fig. 11.

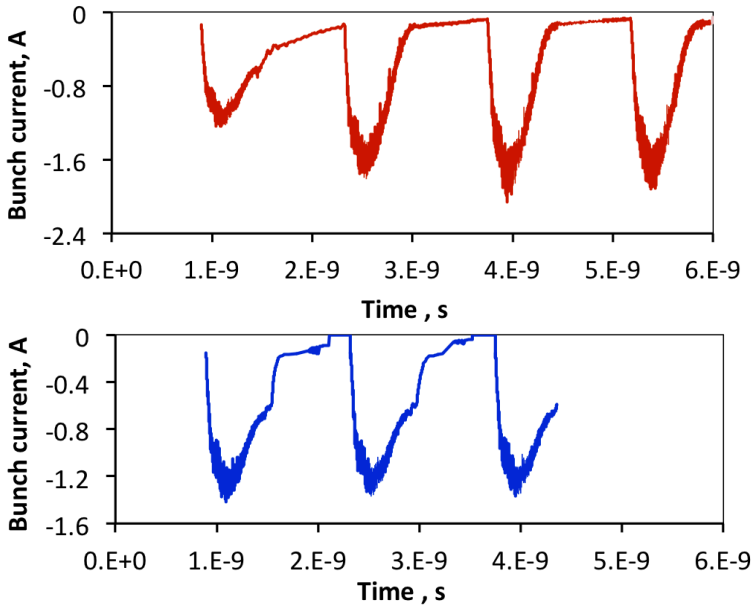


Fig. 12. Comparison of electron bunches at the gun exit with emission from the central hole (top) and without emission from the central hole (bottom).

Figure 12 shows a comparison of the electron bunches at the exit of the gun, with and without emission from the central hole in the cathode. These simulations corresponds to the center and bottom simulations in Fig. 10. The bunch charge with emission from the central hole is 0.77 nC at a peak current of 2.06 A, an RMS bunch width of 166.5 ps, and a FWHM of 374 ps. Without emission from the central hole, the bunch charge is 0.74 nC, the peak current is 1.37 A, the RMS bunch width is 117 ps, and the FWHM is 465 ps, reflecting a more rectangular bunch shape. Note that the interbunch current vanishes completely before the start of the next bunch, once emission from the central hole is removed from the simulation.

Figure 13 shows a summary of the results of slit-based emittance measurements for $V_{cathode}$=-32 kV, $V_{grid}$=-90V, and ~250 W of rf drive at 714 MHz. Except for the values of $I_{lens}$, these experimental parameters correspond closely to the simulations shown in Figs. 10 and 11. The highest value of the measured normalized transverse RMS emittance, as a function of magnet current, is ~15 mm mrad, somewhat lower than predicted by the simulations. Also, the measured emittance drops off at higher values of the magnet current, while the simulations suggest that the emittance should increase. This may result from experimental factors that affect the measurement, including (1) the possibility that electron trajectories through the slit intercept the wall of the vacuum vessel before reaching the YAG screen and (2) effects due to the finite dynamic range of the optical

measurements, which may result in a faint beam halo not being recorded by the measurement system.

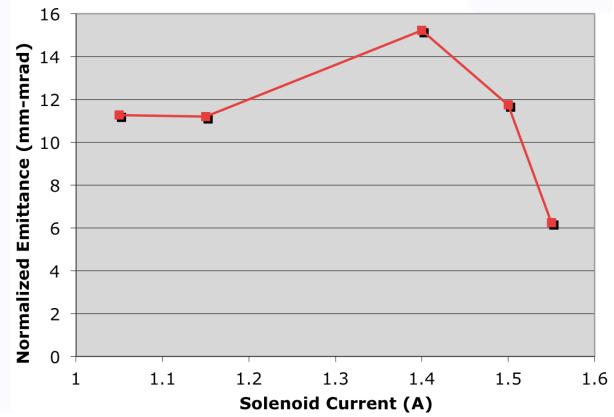


Fig. 13. Measured emittance versus solenoid current for $V_{cathode}$=-32 kV, $V_{grid}$=-90V, and ~250 W of rf drive at 714 MHz.

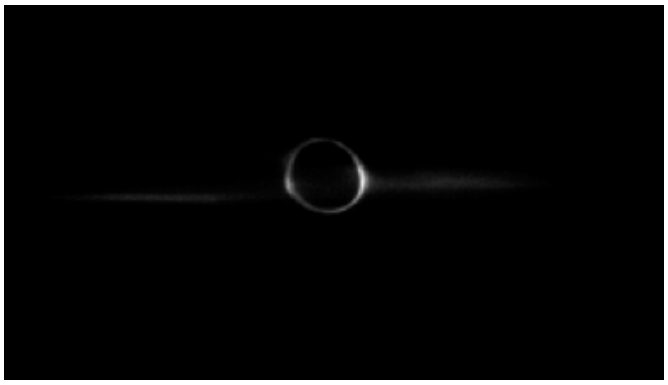

Fig. 14. Image of YAG plate at $I_{lens}$=1.15 A with a 100 μm Ta slit on the beam axis, showing the circular beam pattern resulting from emission through the central hole in the cathode. The faint horizontal line is the result of electron trajectories from the entire cathode as a result of rf drive passing through the slit.

An explanation of the dc current at high values of negative grid bias that are reported from the Faraday cup measurements was provided by optical measurements of the beam that were recorded as part of the slit-based emittance measurements that included the use of a solenoidal lens to collimate the beam. With the slit on or near the beam axis, and a grid bias of -90V, the slit image was measured on the YAG screen at several different values of the magnet current while rf drive was present. In most cases, only the downstream image of the slit was recorded with the transverse spread of the slit image related to the beam emittance. However, at a small range of values of the magnet current, a small circle (~4-mm diam.) appeared on the YAG in addition to the slit image (see Fig. 14); when the rf drive was turned off, only the circle remained. The circle could be brought into sharp focus on the YAG at 1.15 A of solenoid current. This indicated that the source of the electron trajectories should correspond to a well-defined feature on the

cathode whose emission was not strongly suppressed by the negative grid bias. The only candidate feature is the edge of the central hole in the cathode. This region could emit electrons because of barium migration from the face of the cathode, and electron trajectories originating from this region could easily pass through the hole in the center of the grid pattern.

Since the focal length of the lens is known at the electron energy and magnet current employed, and the distance from the lens to the YAG is also known, it is straightforward to calculate the distance to the apparent source of the electron trajectories imaged onto the circle using the thin lens approximation. Using the focal length of the magnetic lens for 32 keV electrons, it was determined that the apparent source of the electron trajectories was ~30 cm behind the cathode, a physical location that clearly cannot emit electrons. The explanation for this is that the electron trajectories emitted from the inner edge of the cathode hole have a strong radial component, but are bent strongly in the vicinity of the cathode until they are close to paraxial straight lines as they exit the gun. The lens formula projects those lines back to their apparent source, which is well behind the plane of the cathode hole.

## 6. Improved electron gun with cathode integrated into the accelerating cavity

The experimental measurements presented earlier in this paper demonstrate the capabilities of a gridded thermionic cathode as the first stage of an electron injector, but also showed that the existing electron gun, which was designed for an entirely different application, falls somewhat short of the typical emittance and bunch length parameters that are required for the FEL application. The same MICHELLE/ANALYST [17, 25] code combination that was used to model the existing gun was also used to design a new improved gun that could be capable of meeting those requirements. Some of the changes are straightforward, such as removing the central hole to eliminate the interbunch current, and reducing the cathode diameter in order to lower the emittance, which requires operating at higher mean emission current density. However, the next step was to envision an electron gun in which the initial DC acceleration between the grid plane and the anode, prior to injection into an rf cavity, is replaced by acceleration using the rf fields of the first cavity. Some preliminary work on this concept was reported in Ref. [26].

The basic concept of this novel rf-gated thermionic electron injector is shown in Fig. 15. It has a cylindrical RF accelerating cavity with the thermionic electron gun mounted in the first end wall on the cavity axis. RF power is fed into the cavity through side power ports (not shown in the picture) and excites the $TM_{010}$ resonant mode of the cavity. The ***E***-field of the mode has its maximum on the cavity axis and accelerates the electron bunches extracted from the cathode through the grid. The gun has a concave spherical cathode and rf modulated grid, with coaxial grid drive for RF excitation of the cathode-grid gap. A positive bias potential $U_0$ relative to the grid is applied to the cathode and prevents emission if no RF excitation voltage $U_1$ is applied across the grid to cathode region. RF excitation of the coaxial grid drive produces rf modulation of the voltage across the cathode beam extraction region. The RF excitation can be the 1st harmonic of the frequency $f$ of the main accelerating

cavity $TM_{010}$ resonant mode or can include higher harmonics of this frequency. To the right of the grid, cavity rf fields accelerate the electron bunches created by the cathode and grid.

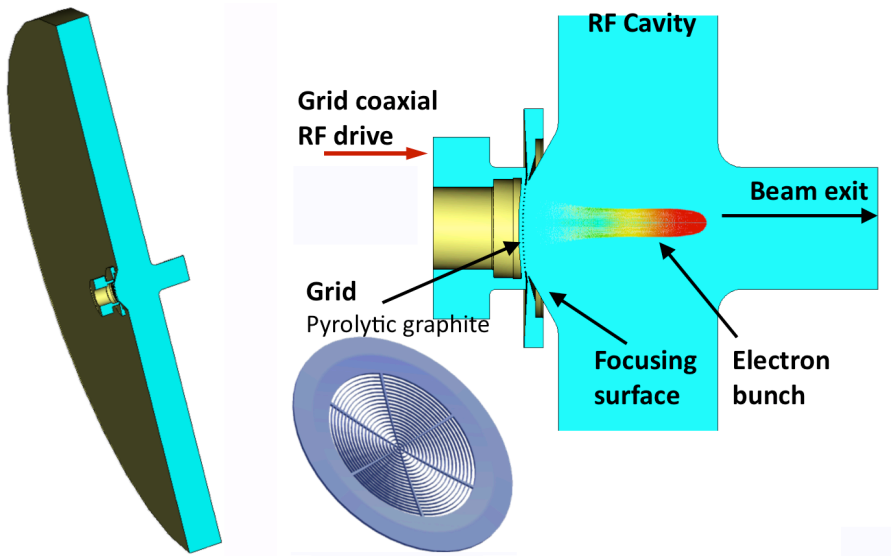


Fig. 15. (Left) Cut-away view of the schematic of a 700 MHz RF-gated thermionic electron gun integrated into a cylindrical RF accelerating cavity. The power port is not shown. (Right) Close-up view of the central region of the cavity, showing the cathode and the holeless grid (inset), and the transit of a electron bunch.

The amplitude $U_n$ of the RF excitation is selected to provide the electric field for extraction of electron bunches of the required charge and duration. Higher positive bias voltage $U_0$ in general leads to shorter bunch duration and also requires higher harmonic RF voltage to keep the bunch charge unchanged. The grid to cathode spacing is selected to keep all the DC and RF $\boldsymbol{E}$-fields below the voltage breakdown threshold. In addition the spacing determines the RF power needed to excite the gap. Our simulations show that the grid to cathode spacing has little effect on the emittances that are attainable. The size of the grid wires affects both the emittance of the electron beam and the structural strength of the grid. A grid with thinner wires produces smaller distortion of the $\boldsymbol{E}$-filed and therefore allows smaller emittance. However, the grid wires must remain thick enough for structural integrity. Pyrolytic graphite is an almost ideal choice for the grid material. It has anisotropic properties, with high metal-like thermal and electrical conductivity in the direction parallel to the grid side surfaces, as well as extremely small thermal expansion.

The key parameters responsible for the bunch properties and control are the DC bias voltage and different combinations of the harmonic amplitudes and phases. This includes the simplest case with only 1st harmonic for the grid RF drive excitation. Higher order harmonics fundamentally allow shorter electron bunches. However, shorter bunches require higher peak currents to achieve the same microbunch charge, and thus either a larger cathode diameter or higher peak

current density from the cathode surface. In turn, a larger cathode diameter will tend to increase the transverse emittance, while operating at higher peak current densities would require operation at higher cathode temperatures, with a negative effect on cathode lifetime. An example of the operation of the new RF-gated bunched thermionic electron gun is shown in Fig. 16, where the beginning stages of the bunch formation are shown. An optimized geometry and optimized bunch extraction RF drive excitation conditions were used in the simulation 700 MHz, with combined first and third harmonic grid drive, to produce about 1 nC of charge with an RMS bunch width of 46 ps, normalized transverse and longitudinal emittances of 11.5 mm mrad and 40.5 kV ps, and an energy of 120 keV.

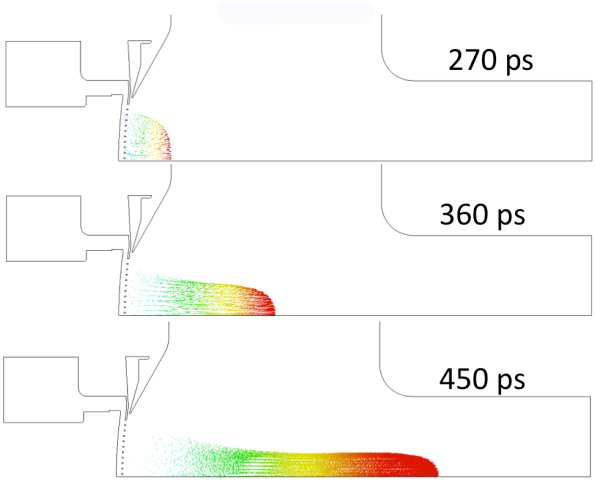


Fig. 16. Beginning stages of bunch formation.

## 7. Conclusions

In this paper, we have presented studies of the performance characteristics of a 35-kV gridded thermionic electron gun in order to evaluate its potential as the prototype for an advanced thermionic electron gun for future FEL injectors. The studies were carried out at 714 MHz, and were used to characterize the electron microbunch charge, microbunch length, and transverse emittance as a function of electron gun voltage, negative grid bias, and rf grid drive, including the effect of adding a third harmonic rf signal to the grid circuit. In studies using a fast Faraday cup, the gun has demonstrated microbunches with a microbunch length of 325 ps FWHM (~135 ps RMS), with 2.81 A peak current and ~0.91 nC per bunch. The use of combined first and third harmonic grid drive has been shown to reduce the length of the microbunches compared to pure first harmonic modulation. We also carried out slit-based measurements of the normalized transverse emittance of electron bunches from the gun, and measured typical values in the range of 10–15 mm mrad. However, these measurements were measured downstream from the gun, and may underestimate the transverse emittance at the gun exit plane due to beam scraping in transport. The emittance and bunch length measurements were compared to the

predictions of detailed simulations using the electron gun code MICHELLE. Both the measurements and the simulations have demonstrated the potential of a gridded thermionic electron gun as the first stage of a high-average current FEL injector, but have also showed that the existing electron gun will need some modifications to achieve the beam parameters required for the FEL application. We also presented an alternative injector configuration with a modified cathode geometry that makes use of direct rf acceleration of the beam from the gridded thermionic cathode. This alternative configuration offers the possibility of improved performance for the intended application.

## Acknowledgments

The authors are grateful for the assistance of L. Chen in developing an image correction software program for the FOculus camera. This work was supported by the Office of Naval Research and the High Energy Laser Joint Technology Office.

References

[1] T. Wangler, *RF Linear Accelerators*, *Wiley Series in Beam Physics and Accelerator Technology*, New York, 1998.
[2] G. R. Neil, C. L. Bohn, S.V. Benson, G. Biallas, D. Douglas, H. F. Dylla, R. Evans, J. Fugitt, A. Grippo, J. Gubeli, R. Hill, K. Jordan, G. A. Krafft, R. Li, L. Merminga, P. Piot, J. Preble, M. Shinn, T. Siggins, R. Walker, and B. Yunn, Phys. Rev. Lett. 84, 662 (2000).
[3] ''Free Electron Laser High Brightness, High Average Current Injector'' report to the NAVY HEL Program Office (PMS-405) & Office of Naval Research,'' P. O'Shea, Panel Chairman, 2002.
[4] A. Todd, Nucl. Instrum. Methods Phys. Res. A 557, 36 (2006).
[5] I. Ben-Zvi and I. V. Bazarov, *Nucl. Instrum. Methods Phys. Res*. A **557**, 337 (2006).
[6] K. L. Jensen, N. A. Moody, D. W. Feldman, E. J. Montgomery, and P. G. O'Shea, *J. Appl. Phys*. **102**, 074902 (2007).
[7] C. Hernandez-Garcia, T. Siggins, S. Benson, D. Bullard, H. F. Dylla, K. Jordan, C. Murray, G. R. Neil, M. Shinn, and R. Walker, in Proceedings of the 21st Particle Accelerator Conference, Knoxville, 2005 (IEEE, Piscataway, NJ, 2005), p. 3117; C. Hernandez-Garcia, P. G. O'Shea, and M. L. Stutzman, *Phys. Today* **61**, No. 2, 44 (2008).
[8] J. Power "Overview of Photoinjectors" *Advanced Accelerator Concepts Workshop 2010,* Annapolis, MD, June 13-19, 2010.
[9] B.E . Carlsten "New Photoelectric Injector for the Los Alamos National Laboratory XUV FEL Accelerator" *Nuclear Instruments and Methods in Physics Research,* North Holland, Amsterdam A285, 1989, pp. 313-319.
[10] A. Yeremian et al., in Proceedings of the 1989 Particle Accelerator Conference, (IEEE, Piscataway, NJ, 1989), pp. 657–659.
[11] J. M. J. Madey, G. J. Ramian, and T. I. Smith, *IEEE Trans. Nucl. Sci*. **27**, 999 (1980).
[12] T. I. Smith, *Physics of Quantum Electronics*, edited by S. F. Jacobs et al. (Addison-Wesley, Reading, MA, 1982), Vol. 8, pp. 77–87.
[13] B. A. Baklakov et al., *Nucl. Instrum. Methods* A 470, 60 (2001); V. P. Bolotin et al., *Nucl. Instrum. Methods* A 557, 23 (2006).
[14] K. Togawa , T. Shintake, T. Inagaki, K. Onoe, T. Tanaka, H. Baba, and H. Matsumoto, *Phys. Rev. ST Accel. Beams* 10, 020703 (2007).
[15] T. Shintake et al., *Phys. Rev. ST Accel. Beams* 12, 070701 (2009).
[16] R. J. Bakker, C.A. J. van der Geer, A. F.G. vanderMeer, P.W. van Amersfoort, W. A. Gillespie, and G. Saxon, *Nucl. Instrum. Methods Phys. Res*. A 307, 543 (1991).
[17] J. Petillo et al., "Recent Developments in the MICHELLE 2D/3D Electron Gun and Collector Modeling Code," *IEEE Trans. Electron Devices Sci*., **52**, no. 5, May 2005, pp.742-748.
[18] P. Sprangle, J. Peñano, B. Hafizi, D. Gordon, S. Gold, A. Ting, and C. Mitchell, *Phys. Rev. ST Accel. Beams* 14, 020702 (2011).
[19] http://www.cpii.com/product.cfm/1/28

[20] E. Wright, K.T. Nguyen, J.A. Pasour, S.J. Cooke, B. Levush, J.J. Petillo, I.A. Chernyavskiy, J.B. DeFord, and B.L. Held, in *Proceedings of the 2009 Particle Accelerator Conference*, Vancouver, BC, Canada, paper TU4RAC03.

[21] "Design and Manufacture of a 120kW CW, 60 kW Minimum 1.3GHz Klystrode® IOT Power Amplifier" Prepared by Y. Li, *European FEL Design Study* EUROFEL-Report-2007-DS5-074, February, 2007.

[22] M. Zhang, "Emittance Formula for Slits and Pepper-pot Measurement," Fermi National Accelerator Laboratory, Batavia, Illinois, FERMILAB-TM-1988, October, 1996.

[23] M. Reiser, *Theory and Design of Charged Particle Beams* (Wiley, New York, 2008).

[24] J. Safranek and P.M. Stefan "Emittance Measurement at the NSLS X-Ray Ring" The Fifth European Particle Accelerator Conference EPAC'96, Sitges, Spain, June, 1996

[25] "3D FEM Analysis software for solving complex problems," by AWR Corp, El Segundo, CA, *Microwave Journal*, vol. 52, no. 7, p. 104, July, 2009.

[26] C. Mitchell, P. Sprangle, and J. Peñano, *IEEE Trans. Plasma Sci*. **40**, 1977 (2012).